J Solid State Electrochem (2012) 16:1077–1089
DOI 10.1007/s10008-011-1490-9

ORIGINAL PAPER

Application of electrochemical impedance spectroscopy in characterization of structural changes of printing plates

Sanja Mahovic Poljacek · Dubravko Risovic · Tomislav Cigula · Miroslav Gojo

Received: 30 March 2011 / Revised: 20 June 2011 / Accepted: 26 June 2011 / Published online: 12 July 2011

Abstract The porous structure of the aluminium oxide surface of lithographic printing plate (PP) has a most significant influence on the quality of the imprints. This study presents the results of application of electrochemical impedance spectroscopy (EIS) in characterization of PPs' porous structures and their changes during chemical processing. Two common PP types—thermal and conventional—were investigated. The influence of the processing solution's working age on topographical changes of PP surface and associated change in the impedance spectra are investigated and discussed. The equivalent electrical circuit models reproducing the observed EIS spectra are proposed. Based on these models two mechanisms of surface's topography changes responsible for degradation of PP performance due to the processing are identified and discussed.

Keywords Printing plate · Aluminium oxide · Anodic film · Pore sealing · Porous structure · EIS

Introduction

Aluminium surface suitable for use as a lithographic printing plate (PP) consists of two different areas: ink-receptive image areas, which carry a photosensitive coating, and fountain solution-retaining non-image areas (aluminium oxide film). In order to improve the fountain solution adhesion on the aluminium oxide film and to enhance the adhesion of the photosensitive coating during the printing process [1, 2], the aluminium foil needs to be roughened by electrochemical processes of graining and anodic oxidation [3–6]. These processes ensure the formation of specific anodic layer on the aluminium foil which consists of a thin nonporous compact oxide layer (barrier layer) and an outer extremely porous oxide layer. Size and quality of the grained microstructure, i.e., of the porous layer will influence the printing performance and durability of the PPs [7, 8]. Consequently, the porous structure of the lithographic PP has a most significant influence on the quality of the imprints because the adsorption of the fountain solution on the nonprinting elements prevents the adsorption of printing ink on those areas during reproduction process.

The photoactive coating, after exposure in the PP making process, becomes soluble in the alkaline solution. Alkaline solution (pH≈13) mainly based on sodium or potassium hydroxides is used to remove this coating from nonprinting parts of the PPs, supposedly without significantly affecting the structure of the aluminium oxide layer. Nevertheless, the amorphous structure of the aluminium oxide can be affected by such chemical processing [9], inducing changes that impair the quality of the PP. The extent of these undesirable effects presumably also depends on the working age of the processing solution. The immersion of the aluminium oxide porous layer into the alkaline solution as required by processing technology could change the topography of the porous layer and consequently result in degradation of the PP performance. This kind of structural changes influencing the functional properties of the PPs could occur as a consequence of (pore) sealing process [9]. Hence, as the adsorption, i.e., the technological performance of a PP, depends on the porosity of aluminium oxide structure, characterization of this

S. Mahovic Poljacek (✉) · T. Cigula · M. Gojo
Faculty of Graphic Arts, University of Zagreb,
Getaldiceva 2, HR-10000 Zagreb, Croatia
e-mail: smahovic@grf.hr

D. Risovic
Molecular Physics Laboratory, Ruder Boskovic Institute,
POB 180, HR-10002 Zagreb, Croatia

porous structure and estimation of processing influences are of considerable interest and technological importance. Although the successful application of electrochemical impedance spectroscopy (EIS) for characterization of different porous surfaces showing good and reproducible results has been reported previously [10–14], so far EIS has not been used for the characterization or quality control of the lithographic PPs.

In this study, we present the results of application of EIS in characterization of PPs' porous structures and propose models of the equivalent electrical circuits reproducing the observed EIS spectra. The influence of processing solution's age on topographical changes and associated change in impedance spectra are considered and discussed.

Experimental details

Materials

The lithographic PPs used in this study are 0.3-mm-thick AA1050 aluminium foils (also containing 0.05–0.25% Si, 0.30–0.40% Fe, 0.10–0.30% Mg, max 0.05% Mn, and max 0.04% Cu, [15]) comprising two different areas: ink-receptive image areas, which carry a photosensitive coating, and fountain solution-retaining non-image areas (aluminium oxide). For technological purposes [2, 16, 17], the foil's surface is roughened by electrochemical graining and anodic oxidation [1]. Surface structure differences and roughness of the non-image areas of the PP depend on PP type and are a result of different manufacturing methods, which include chemical and electrolytic graining processes as explained in the literature [1, 3–5].

In this study, we have used samples of two PP types: thermal printing and conventional PPs, which are designated by letters A and C, respectively. The thermal PPs were Agfa Thermostar P970, and the conventional PPs are Cinkarna Kemolit PO7.

Preparation of the samples and test procedure

The reference samples (hereafter designated A0, and C0) which were used in the experiments were "raw" PP aluminium foil, i.e., subjected only to graining and anodization [3–6] but without any post-processing. Other samples, initially identical to the reference samples, following the standard procedures, were firstly exposed to defined irradiation (samples A, infrared [IR] laser; samples C, ultraviolet [UV] exposure), and then processed in order to chemically remove the photosensitive coating from the non-image areas of the PPs. The removal was achieved by chemical processing in alkaline solutions (pH≈13) [18, 19] prepared according to the standardized procedure [16, 17]. Each PP sample was processed at the solution temperature of 22±3 °C, processing speed in the range of 0.9–1.3 m/min and the processing time (duration of the PP immersion in the alkaline solution) of 22±4 s.

To assess the influence of working age of the solution used for chemical processing on the topography of PP surface the chemical processing of initially identically prepared samples was carried out in alkaline solutions of different working age: from freshly prepared solution (sample designated A1, C1) up to 84-h-old solution (A8, C8). Quality control of all PP samples was compliant to the graphic technology standards [16, 17], and conducted after the processing. The influence of solution working age on processing was checked on samples selected at 12-h intervals of solutions usage. The process of selecting and analyzing the plates was terminated after the selected PP did not comply any more with the demands of the pertinent quality standards.

Test method and equipment

EIS measurement of the PPs were performed by the immersion of the samples in unstirred, aerated 3.5% (*w/w*) K_2SO_4 solution at 30 °C, according to the procedure detailed in Refs. [8, 12–14, 16, 17, 20]. The area of the samples exposed to the solution was 1 cm^2. The electrochemical cell consisted of Ag│AgCl reference electrode, platinum counter electrode and working electrodes (anodized aluminium sheet). Electronic equipment comprehended an EG&G Lock-in-amplifier Type 5210 in combination with an EG&G Potentiostat/Galvanostat Type 263 A at an open circuit potential. EIS spectrum was measured over the frequency range of 10 mHz to 100 kHz under controlled potentionstatic conditions. Capacitance and resistance data were obtained by software PowerSine EIS Software Equivalent Circuit [21] and the equivalent circuits' fits to the experimental data were accomplished using PAR ZSimp software [22].

SEM micrographs of the investigated samples were obtained with JEOL JMS T300 scanning electron microscope. To ensure the uniform electrical properties and to avoid the charging/discharging of aluminium oxide surfaces, the aluminium plate samples 5×5 mm were gold-coated (>30 nm thick) by magnetron sputter SC7620 Quorum Technologies, Polaron.

The roughness parameters were measured by electromechanical profilometer Perthometer S8P (Mahr GmbH, Göttingen) with a diamond stylus of 2 μm radius. During the measurement, the stylus was moved at a constant speed across the samples with a measuring force of 0.4 mN.

The estimation of fractal dimension of the SEM images was carried out using Fractal3e analysis software [23] using the methods described previously [24].

Results and discussion

SEM

The SEM micrographs presented in Fig. 1 show structures of the aluminium oxide surfaces of the reference, untreated PP samples of thermal and conventional PP types at different magnification. The untreated (reference) samples of thermal and conventional PP are designated A0 and C0, respectively. It can be seen that the aluminium oxide surfaces of the respective reference samples are characterized by dissimilar, inhomogeneous microstructure. These different structures are a consequence of different electrochemical graining procedures applied in the production as described elsewhere [1, 3, 4].

The surface structure of the A0 sample is relatively flat without any pronounced peaks containing numerous densely packed and relatively shallow oval pits whose size is less than 10 μm. A higher magnification reveals rather sharp pit edges. The surface of the C0 PP is more granular, characterized with deeper almost circular pits/pores of different sizes separated with connected ridges and peaks. At higher magnification, smaller microstructures contained within the wider pits can be noticed. In average the surface is significantly rougher than that of sample A0. This is also corroborated with the values of the respective profilometric parameters listed in Table 1.

The definitions of the listed parameters are as follows: R_a, average surface roughness; R_{pm}, mean value of leveling depths (distances between highest peak and reference line); R_z, mean value of single roughness depths and R_{pm}/R_z ratio providing information about the shape of the surface profile, can be found in the pertinent standard and literature [24, 25]. In this study, it is noteworthy that the higher values of the R_{pm}/R_z ratio correspond to "spikier" surface roughness profile, while the lower values correspond to more rounded and flat profiles. Although there are significant differences in the values of roughness parameters the small difference in the R_{pm}/R_z ratio indicates that the shape of the surface profile of two PP types is similar. This is corroborated with practically identical values of the corresponding fractal dimensions D (A0)=2.41 and D(C0)=2.39. Further and more detailed analysis of roughness parameters and their changes with processing are outside the scope of this study.

In Fig. 2, SEM micrographs of PP samples chemically processed in alkaline solution of different working (usage) age are presented. A1 and C1 correspond to the samples processed in a freshly prepared solution; A7 and C7 were processed with the solution of 72 h working age; while samples A8 and C8 were processed in an 84-h-old solution. After the selection of A8 and C8 PP samples, other samples selected at latter times of solution usage, i.e., higher working age did not comply any more with the requirements of the pertinent PP quality standards.

The comparison of SEM micrographs of unprocessed (Fig. 1) and processed samples depicted in Fig. 2 shows that the processing causes significant changes of the surface structures of both PP type samples. With processing, the structure of A samples becomes more homogeneous, and the size of pits decreased but they remained isolated and unconnected. The pores became shallower and the walls thicker, without sharp edges. Microstructure of this sample (A1) is more uniform than that of the reference sample (A0) and it is dotted with smaller pits separated by connected

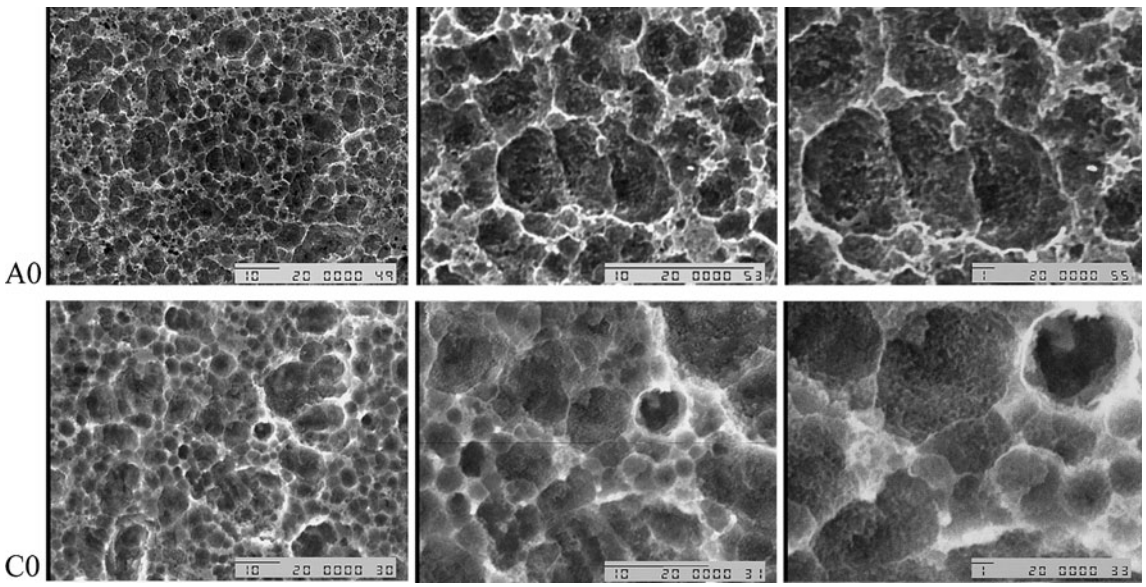

Fig. 1 SEM micrographs of the reference plate samples A0 (thermal PP) and C0 (conventional PP), at magnification ×1,500, ×3,500 and ×7,500, respectively

Table 1 Profilometric parameters of reference and treated samples

Parameter (stylus)	Reference (untreated) sample		Processed sample	
	A0	C0	A1	C1
R_a (μm)	0.59	1.13	0.52	0.78
R_{pm} (μm)	1.66	3.50	1.45	2.11
R_z (μm)	4.54	8.76	4.02	5.54
R_{pm}/R_z	0.37	0.40	0.36	0.38

ridges. These changes are reflected in decreased values of roughness parameters of sample A1 with respect to those of *A*0 (see Table 1). Analysis of SEM images of samples processed in aged solutions (A7 and A8) reveals a practically complete disappearance of peaks, significant sealing of pores and occurrence of plateaus/terraces of redeposit material. Decrease in roughness involving diminishing of deep pits and formation of plateaus dotted with small pores can be clearly seen. Such topography could be the result of dissolution of sharp peaks and sealing of pores with dissolved material, and/or deposition of the material from the solution that has been used for a long time.

Considering the SEM images of conventional PPs, it can be seen that processing even in fresh solution results in significant closing of initially relatively deep and narrow pores (cf. Fig. 2, C1). In comparison to the reference (untreated sample), the surface is significantly more homogeneous and flat, which is also reflected in significant reduction of roughness parameters. The results of processing with "older" solutions results in what seems to be less homogenous and somewhat granular surface (cf. Fig. 2 C7). Processing in yet older solution results in surface topography characterized by shallow pits surrounded with broader, connected flat ridges but with no visible terrace-like structures (C8).

In general, chemical processing of PP causes various microstructural changes in the topography of porous aluminium oxide layer. These changes depend on the age of processing solution and eventually lead to degradation of the surface structure from its original–optimal roughness. The resulting changes illustrated here, depend on PP type and have been previously quantified by different roughness measurements techniques and fractal analysis of SEM images [24]. However, although they provide valuable information on change of the surface topography and correlations between profilometric and EIS parameters and the corresponding fractal dimension, these analyses [26, 27] did not consider the possible mechanisms causing the observed changes.

On the other hand, the processing in an alkaline solution influences and changes the dielectric properties of the aluminium oxide surface of a PP and results in changes of the corresponding impedance spectrum thus providing additional means of characterization of topographical changes of PP surface.

EIS

Considering the structure of specific anodic layer on the aluminium foil, which consists of a thin nonporous compact

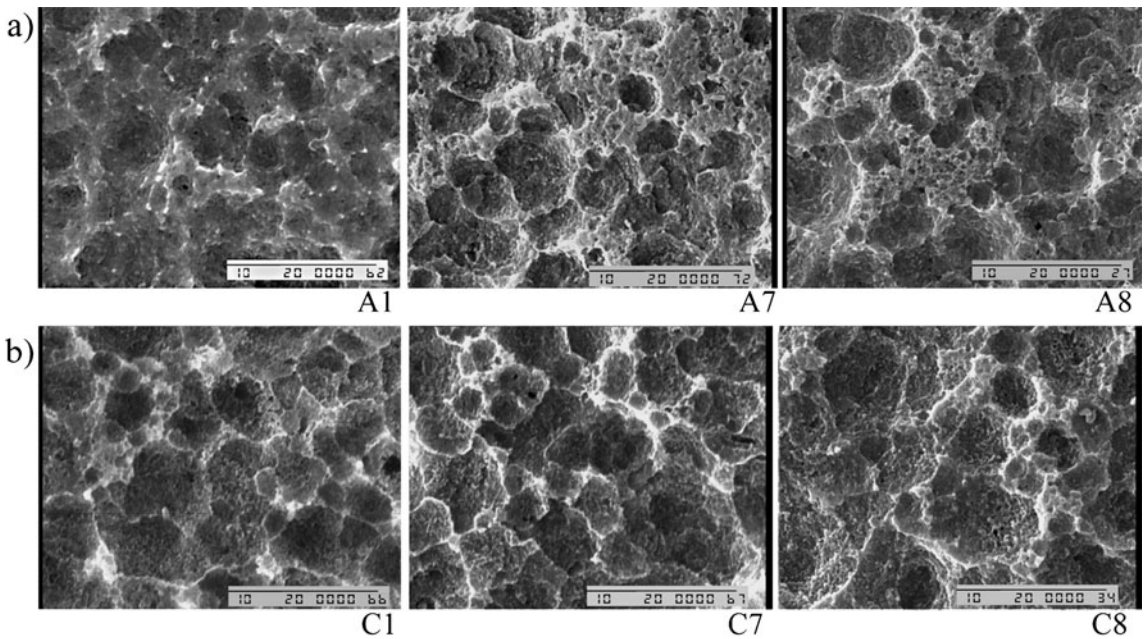

Fig. 2 Printing plate samples processed in alkaline solution of different working age: freshly prepared solution (A1 and *C*1); 72 h (A7 and C7) and 84 h (A8 and C8). Magnification ×5,000

oxide layer (barrier layer) and an outer extremely porous oxide layer, we arrive at physical model of the interface. The pores extending from surface to the barrier layer are separated by pore walls and filled with electrolyte/processing solution. This situation corresponds to the simple open pore model. During the processing, the possible mechanisms influencing the surface roughness and interface structure are dissolution and (in case of multiply used of solution) possible re-deposition of dissolved material from the solution. The dissolved material may partially or fully fill the pores and form an intermediate layer on the surface. Such situation is described by the (partially) sealed pore model.

Rough schematics of the general interface structure corresponding to the described physical model with superimposed corresponding equivalent circuit (EC) model(s) used in this study are depicted in Fig. 3. Similar models were used previously for the description and study of porous oxide layers [11, 29–35].

From these general models, simplified models adequate for description of open pore can be readily derived. The results of EIS measurements and equivalent circuits modeling performed on the reference samples of the thermal PP (A0) and the conventional PP (C0) are presented in Figs. 3 and 4. According to the de Levie theory [28], the shape of recorded Nyquist plot for A0 sample, i.e., almost perfect semicircle (lower curve in Fig. 4), corresponds to a surface structure with shallow pores, while that of C0 sample—a somewhat skewed/compressed semicircle (upper curve in Fig 4)—corresponds to a surface with deep pores. This is in agreement with the surface structures revealed in SEM micrographs of the reference samples (cf. Fig. 1).

Figure 5a and b shows the corresponding Bode (phase and modulus) plots of the measured and modeled data for the reference samples A0 and C0, respectively. The moduli vs. frequency curves exhibit the behavior typical for open porous structure. However, occurrence of a very small dip in the phase angle curve at moderate frequencies observed for the A0 sample could be interpreted as a sign of a slightly partially sealed porous structure: A pronounced dip in the phase angle curve at moderate frequencies is a characteristic corresponding to the partially sealed structure. Such dip is absent in the phase Bode plot corresponding to the conventional PP, indicating completely open pores clearly seen in the SEM micrographs.

The calculated data shown in Figs. 4 and 5 indicate that the measured EIS data for both samples can be well modeled with the equivalent circuit of a Voigt type $R(QR)(QR)$, containing two capacitive loops (Fig. 6a). Such

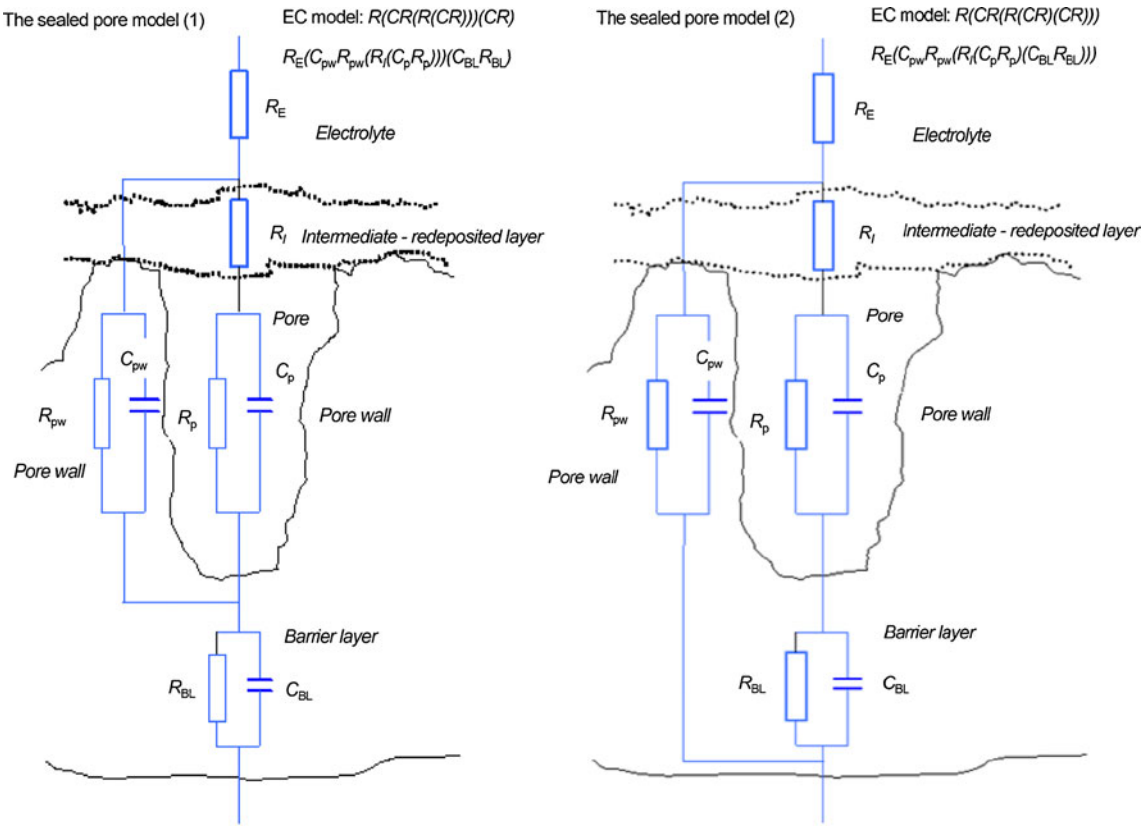

Fig. 3 Schematics of the interface structure with superimposed EC corresponding to two closed pore models used in the investigation

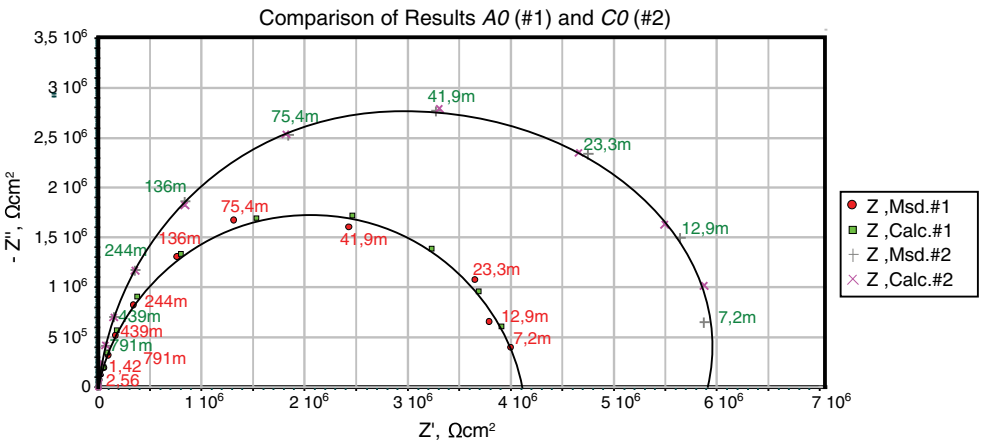

Fig. 4 Nyquist plots of measured and modeled data for the reference samples A0 (thermal PP) and C0 (conventional PP). Symbols represent measured and EC modeled values and lines the corresponding fit. The calculated values are obtained based on *R*(*QR*)(*QR*) equivalent circuit model

circuit corresponding to a simple physical model of an open pore is also often used to model the oxide films [29–31] and represents a simplification of a more general model used for description of behavior of anodic films [32]. This EC is experimentally indistinguishable from the model based on previously proposed structure of the porous oxide

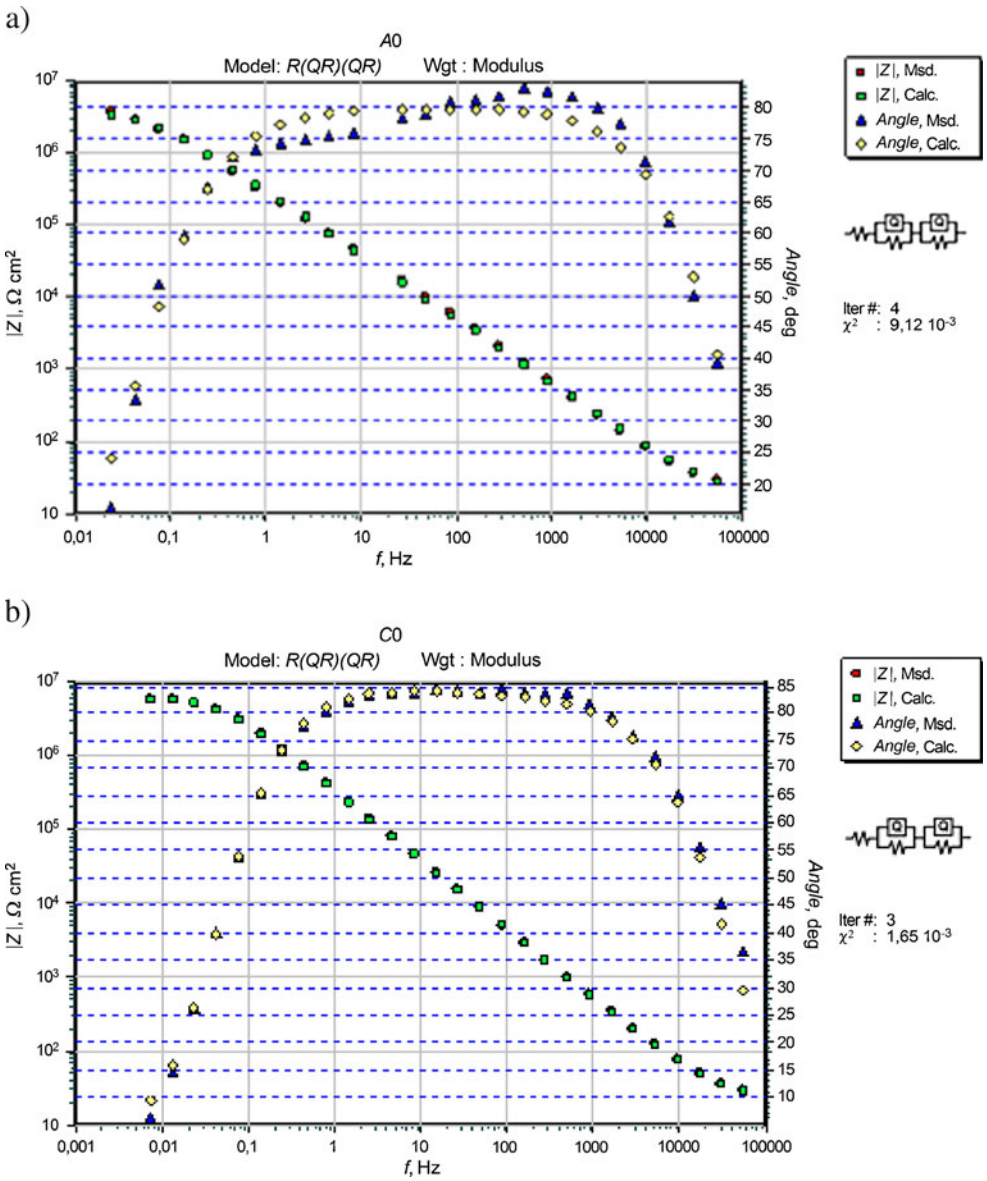

Fig. 5 Bode plots of measured and modeled data for the reference samples **a** A0 (thermal PP) and **b** C0 (conventional PP). The calculated values are obtained based on *R*(*QR*)(*QR*) equivalent circuit model. The values of the EC elements are given in Table 2

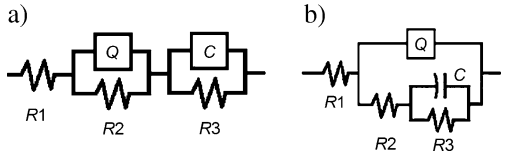

Fig. 6 **a** Equivalent Voigt type circuit $R(QR)(CR)$, corresponding to the simplified physical model of an open pore structure. **b** Corresponding ladder type circuit $R(Q(R(CR)))$. R_1 solution resistance, R_2 pore electrolyte and intermediate layer resistance, Q constant phase element, C capacitance, R_3 resistance of the barrier layer

layer [11, 33–35] depicted in Fig. 6b. This simple open pore EC is derived from the general sealed pore model depicted in Fig. 3 by removing the intermediate layer and assuming that the resistance of the pore wall is very high in comparison to the pore resistance.

However, for both models instead of the simple capacitance in the pore branch of the ECs we have introduced a constant phase element (Q) to include the possible effects of fractal nature of the considered structure [27]. The impedance of a constant phase element is given by:

$$Z(Q) = \frac{1}{C(i\omega)^n}$$

where ω is the frequency and n is the frequency dispersion parameter related to fractal dimension of the structure.

The values of the EC parameters obtained by best fit to the experimental data of A0 and C0 samples (cf. Figs. 4 and 5) are presented in Table 2. The values are rounded to significant digits.

The values of the EC parameters of a simple open pore model corresponding to A0 and C0 samples, obtained from the fit to the experimental data point to slight differences between the two PP types. In particular, the differences in the pore resistance and resistance of the barrier layer indicate that the conventional PP has narrower pores and somewhat thicker barrier layer. The difference in the exponent n_p of the constant phase element Q indicating the difference in the fractal dimensions of the surface/pore structures between the PP types is probably too high. That is, based on the value of fractal dimension determined from corresponding SEM images ($D \approx 2.4$ for both samples, implying $n \approx 0.72$), one would expect smaller difference in n_p between the samples. This greater difference may result from errors in fit or indicate the slight influence of some other process e.g. semi-infinite diffusion.

Table 2 Values of EC parameters for the simple open pore models

Sample	A0	C0
Model	Simple open pore $R(QR)(QR)$	Simple open pore $R(QR)(QR)$
Parameter		
χ^2	9.124×10^{-3}	1.655×10^{-3}
R_S (Ω cm^2)	17.5	22
C_p/Q_p (F cm^{-2})/(S s^n cm^{-2})	2.1×10^{-5}	9.5×10^{-5}
n_p	1	0.63
R_p (Ω cm^2)	112	489
C_b/Q_b (F cm^{-2})/(S s^n cm^{-2})	6.6×10^{-7}	5.2×10^{-7}
n_b	0.89	0.94
R_b (Ω cm^2]	4.2×10^{6}	6.1×10^{6}

Generally, the processing of PPs should not have adverse effects on its surface structure, i.e., not impair its performance. However, the structure of the PP surface does change in processing and this change is related to the working age of particular processing solution. SEM micrographs show that in comparison with untreated samples the change of surface structure is more pronounced after processing in aged solution (cf. Fig. 2). The Bode plots obtained by EIS for PPs processed with freshly prepared solution are depicted in Fig. 7. By comparing these plots with those of the reference samples (Fig. 5), it can be seen that the processing with freshly prepared solution indeed affects the surface pore structure. The change in corresponding Bode plots is not so much qualitative (i.e., in shape of curves) as it is quantitative. The influence of processing is more pronounced in thermal PP. The largest difference between the PP types and their response to the processing is manifested in significant (one order of magnitude) decrease in impedance modulus of the thermal PP at low frequencies, accompanied by decrease in magnitude of the phase angle in the intermediate frequency range.

The observed changes in EIS data due to processing in freshly prepared solution can be more or less satisfactory modeled by the simple open pore EC depicted in Fig. 6. However, much better agreement with the measured EIS data is obtained using the model of partially sealed or closed pore (Fig. 7). We have investigated two possible models for a closed pore structure depicted in Fig. 3. These slightly more complicated models were developed from the basic open pore model $R(Q(R((CR)))$ depicted in Fig. 6b. Slightly better performance, i.e., compliance with experimental data was achieved with the (partially) sealed pore model (2). This is a $R(CR(R(QR)(QR)))$ model depicted in the Fig. 8. Here, aside from including the pore wall capacitance and resistance into the EC, another resistance (R_2) was introduced to take into account formation of an intermediate layer on the surface of the porous layer formed by the deposited material from the solution. In addition, to allow for the changes in the barrier due to the interaction with the processing fluid, a CPE element was introduced instead of the simple capacity.

The fitting procedure for such relatively complex model could be demanding, and sometimes a good fit to experimental data can be obtained with values of parame-

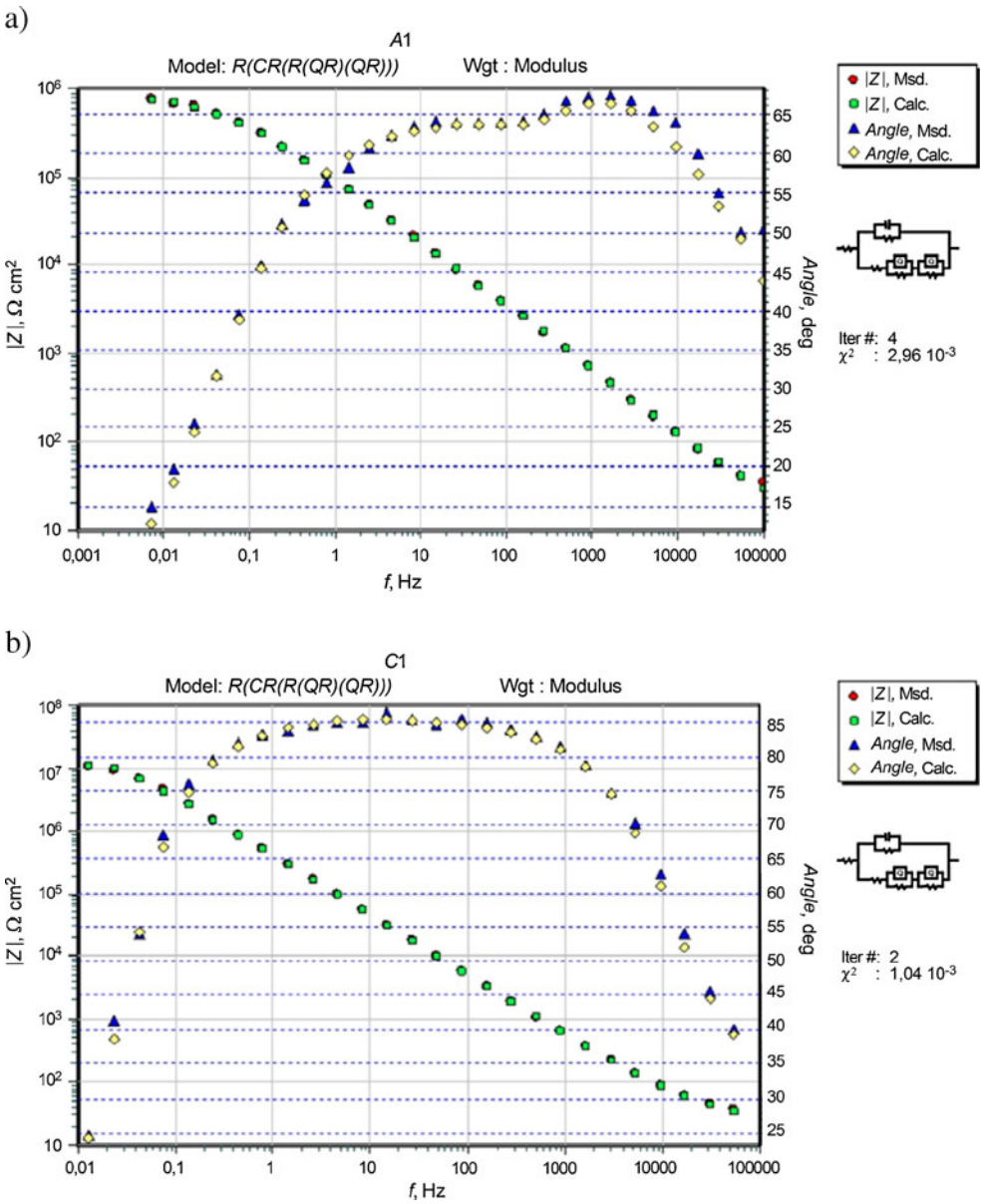

Fig. 7 Bode plots of measured and modeled data for the PP samples processed in freshly prepared solution: **a** thermal PP sample and **b** conventional PP sample. The calculated values are obtained based on the sealed pore model (2), i.e., $R(CR(R(QR)(QR)))$

ters that are physically unrealistic. To avoid such pitfalls, in fitting procedure we have limited the range of some parameters to physically realistic values obtained from calculations and/or physical considerations. For example,

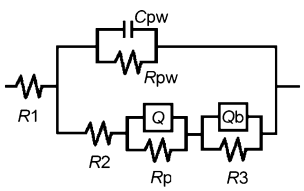

Fig. 8 Equivalent circuit $R(CR(R(QR)(QR)))$ corresponding to the physical model of porous structures with partially sealed pores. R_1 solution resistance, R_2 resistance of the intermediate layer (pore cover), R_3 barrier resistance, Q constant phase element. Subscripts "p" and "pw" indicate quantities corresponding to the pore and pore wall, respectively

the electrolyte resistance is low, while the barrier resistance is high and depends on its thickness (that is approximately known) and cannot be smaller than the pore resistance, etc.

The values of EC parameters corresponding to the simple open pore and closed pore models applied to thermal and conventional PP after the processing in freshly prepared solution are summarized in Table 3.

Analysis of the data presented in the Table 3 indicates that the thin intermediate layer of low resistance has been formed on the surface of both samples, and that the processing resulted in partial filling of shallow pores (sample A) and practically complete closing of the initially narrower and deeper pores (sample C).

Generally, when PP samples are immersed in the processing solution, the fluid may be absorbed into the pores of the surface structure causing two opposing effects

Table 3 Values of EC elements for simple open pore and closed pore models

Sample	A1		C1	
Model	Simple open pore	Closed pore (2)	Simple open pore	Closed pore (2)
Parameter (EC)	$R(QR)(QR)$	$R(CR(R(QR)(QR)))$	$R(QR)(CR)$	$R(CR(R(QR)(QR)))$
χ^2	5.102×10^{-3}	2.962×10^{-3}	4.909×10^{-3}	1.036×10^{-3}
R_S (Ω cm^2)	15	15	20	17.5
C_{pw}/Q_{pw} (F cm^{-2})/(S s^n cm^{-2})		5.7×10^{-8}		8.8×10^{-8}
n_{pw}				
R_{pw} (Ω cm^2)		9.8×10^{5}		2.0×10^{7}
R_I (Ω cm^2)		42.7		45.1
C_p/Q_p (F cm^{-2})/(S s^n cm^{-2})	3.9×10^{-6}	2.1×10^{-6}	7.2×10^{-6}	2.2×10^{-6}
n_p	1	1	0.73	0.80
R_p (Ω cm^2)	200	186.2	9.7×10^{4}	3.0×10^{5}
C_b/Q_b (F cm^{-2})/(S s^n cm^{-2})	2.8×10^{-6}	2.8×10^{-6}	4.2×10^{-7}	3.6×10^{-7}
n_b	0.73	0.70		0.99
R_b (Ω cm^2)	8.4×10^{5}	9.1×10^{6}	1.2×10^{7}	3.2×10^{7}

previously observed in anodized films [36, 37]: self-sealing and deterioration. Depending on the particular processing fluid and PP type, one phenomenon/process prevails over the other. In the first process the anhydrous alumina reacts with absorbed water, which leads to voluminous hydrated alumina resulting in a self-sealing effect. Thus, the resistance of the porous layer increases. The self-sealing mechanism involves degradation, gelling, agglomeration and a precipitation process [38]. As there is a reduction of free water content inside the pores because of the formation of hydrated alumina, and the permittivity of the hydrated alumina is lower than that of free water, the value of Q obviously decreases.

At the same time, the anodic film may also, to some extent, be attacked by aggressive ions from the processing solution [39]. The conversion of alumina to hydrated alumina may be retarded because of the aggressive ions in the solution. Thus, the resistance of the porous layer decreases and capacitance of the porous layer increases.

The analysis of the changes in EC's elements used to fit the experimental data indicate that the first mechanism is responsible for the changes observed in processed thermal PP samples, while the other mechanism is dominant in processing of conventional PP.

The effect of solution working age on PP surface structure is best seen in the Bode phase plots depicted in Figs. 9 and 10. The phase plots of thermal PPs (Fig. 9) show the occurrence of a dip at middle frequencies that increases with the working age of processing solution.

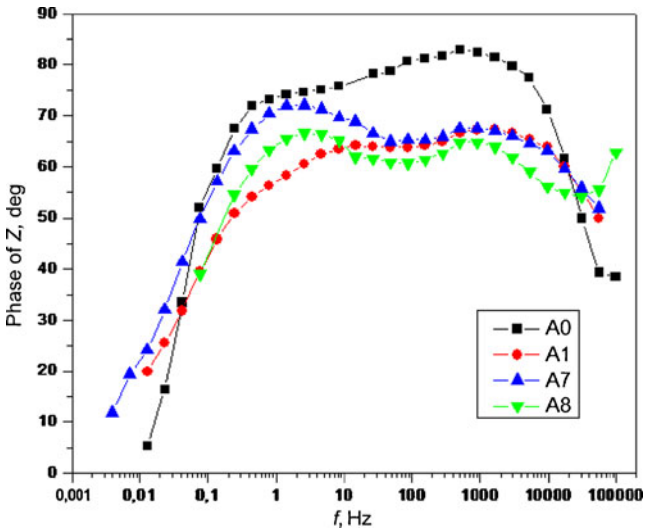

Fig. 9 Bode phase plots of the thermal PP samples processed in solutions of different working age. The *symbols* represent the measured data and line the corresponding B-spline fit

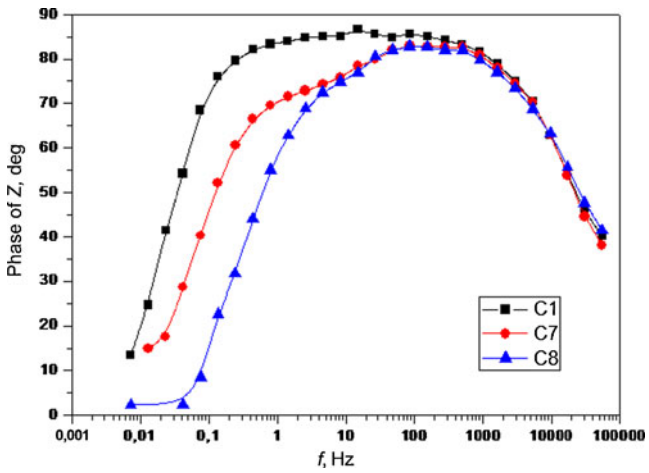

Fig. 10 Bode phase plots of the conventional PP samples processed in solutions of different working age. The *symbols* represent the measured data and line the corresponding B-spline fit

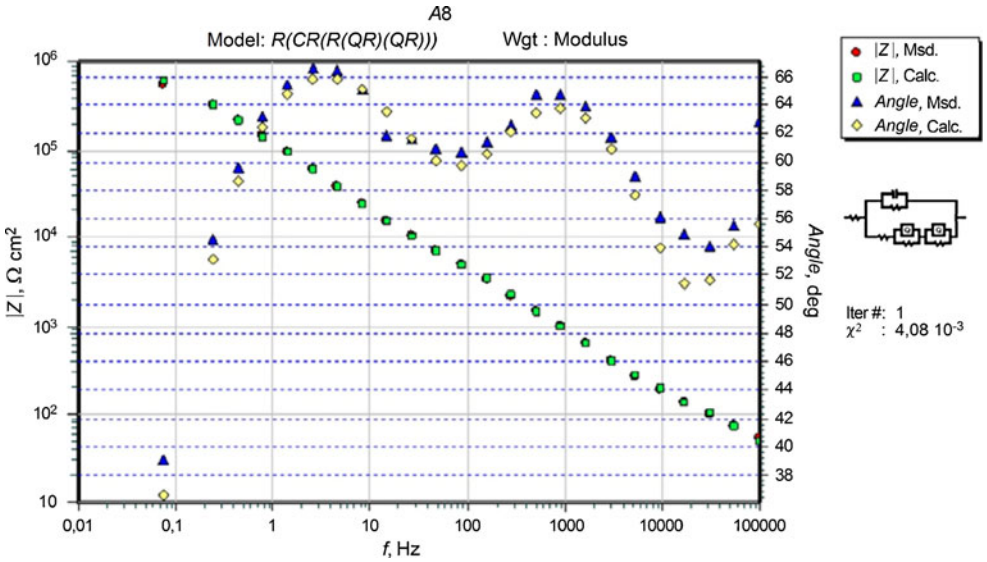

Fig. 11 Bode plots of measured and modeled data for the thermal PP sample A8 processed in aged solution. The calculated values are obtained based on partially sealed pore equivalent circuit model $R(CR(R(QR)(QR)))$

Occurrence of such dip is a characteristic of a sealing process, i.e., closing of the pores. The dip increases with the processing solution working age, and is not observed in phase plots corresponding to samples processed with freshly prepared solution. Also, the slight increase in the impedance values of the samples processed with solutions of different working age in respect to those corresponding to the sample processed in fresh solution, indicates an increase of the layer thickness. Hence, we conclude that the pore sealing is caused by re-deposition of the material from the processing solution. These changes in Bode phase plots are accompanied by relative increase of impedance modulus at medium and higher frequencies. Such behavior was previously observed in hydrothermal sealing process of anodized layers [40–42].

The Bode plots of conventional PP, depicted in Fig. 10, show that the phase plots are distorted by decreasing the phase angle not only at middle frequencies, but also at the side of low frequencies. The values of phase angle at the high frequency side remain practically unchanged, i.e., not influenced by solutions working age. The main changes occurring at lower frequencies indicate deterioration of the oxide layer caused by interaction with aged processing solution.

The observed differences in behavior of conventional PP in regard to the thermal PP are the consequence of different electrochemical conditions in which the graining and anodic oxidation processes have been performed resulting in initially different surface structures. Moreover, the chemical processing of exposed PP is performed in different developers. In order to model the measured EIS data two ECs corresponding to the sealed pore models were applied (cf. Fig. 3). Slightly better performance, i.e., compliance with the experimental data was achieved with

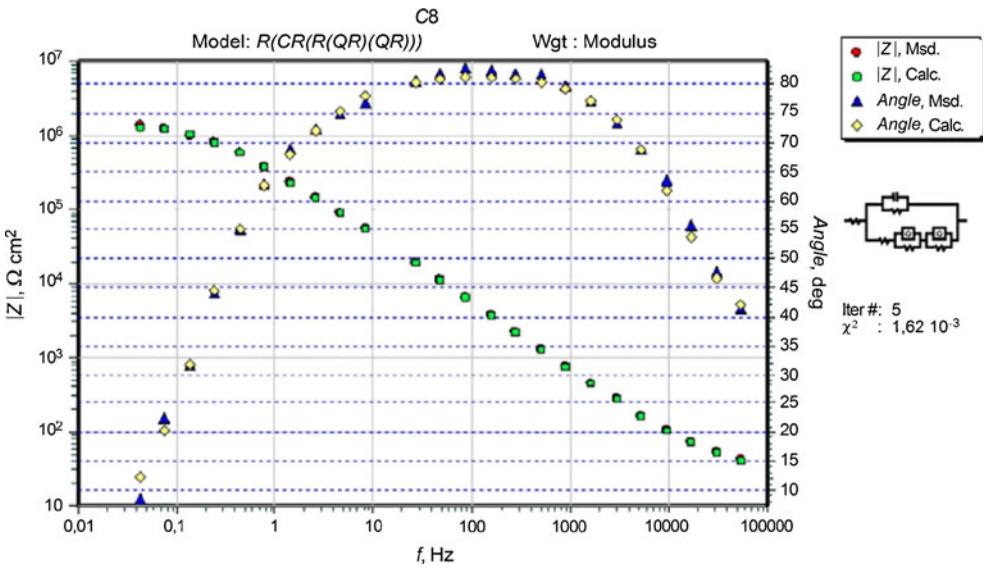

Fig. 12 Bode plots of measured and modeled data for the conventional PP sample C8 processed in an aged solution. The calculated values are obtained based on partially sealed pore equivalent circuit model $R(CR(R(QR)(QR)))$

the (partially) sealed pore model (2), i.e., with a $R(CR(R(QR)(QR)))$ model depicted in the Fig. 8.

The results of measured Bode plots of samples A8 and C8 together with results obtained with the EC model from Fig. 8 are depicted in Figs. 11 and 12, respectively. The values of the parameters of the corresponding ECs are given in the Table 4.

The Bode plot of thermal PP sample processed in aged solution exhibits strong dip in the phase curve, characteristic for pores that are completely sealed with deposited material from the solution. Low phase angle values without any line segments indicate strong deviation from the capacitive behavior. The impedance modulus linearly decreases with frequency in the whole frequency range.

Aside from a significant (1 order of magnitude) lowering of the impedance modulus and phase angle at low frequencies, the Bode plot corresponding to the conventional PP processed with an aged solution (Fig. 12) does not exhibit any pronounced signs corresponding to partial sealing of the pores with different material noted in thermal PP samples.

This is the consequence of different manufacturing and anodization processes of conventional PP and different processing solution. Although the equivalent circuit is the same as in the case of thermal PP sample, the values of the corresponding EC's parameters shown in Table 4 are different. The resistance of the pore plug is a few orders-of-magnitude higher than the corresponding values of for the filling material in case of thermal PP. Compliant with this are the corresponding values of the CPE exponents is higher than that corresponding to the thermal PP sample, indicating relatively compact filling of the pore, in contrast to the more porous fractal structure of the thermal PP pore-filling material characterized by significantly lower n.

However, in both samples, the C_p is much higher than C_{pw}, and decreases with closing of the pore as observed before [11].

Generally, one may say that the composition and characteristics of the hexagonal cell walls and barrier layer are similar if not the same for both PP types. On the other hand, the pore structure and changes induced by processing, such as the extent of pore's filling and its composition, are different and PP type–dependant.

Figure 13 shows the overall variation of relevant EC parameters with working age of processing solution for

Table 4 Values of EC elements of closed pore models corresponding to samples A8 and C8

Sample Model Parameter (EC)	A8 Closed pore (2) $R(CR(R(QR)(QR)))$	C8 Closed pore (2) $R(CR(R(QR)(QR)))$
χ^2	4.081×10^{-3}	1.620×10^{-3}
R_S (Ω cm^2)	15	17.5
C_{pw}/Q_{pw} (F cm^{-2})/(S s^n cm^{-2})	3.3×10^{-8}	6.6×10^{-8}
n_{pw}		
R_{pw} (Ω cm^2)	1.1×10^{6}	1.4×10^{6}
R_I (Ω cm^2)	125.1	51.9
C_p/Q_p (F cm^{-2})/(S s^n cm^{-2})	2.7×10^{-6}	1.8×10^{-6}
n_p	0.76	0.82
R_p (Ω cm^2)	2558	1.1×10^{5}
C_b/Q_b (F cm^{-2})/(S s^n cm^{-2})	1.9×10^{-6}	5.2×10^{-7}
n_b	0.78	0.93
R_b (Ω cm^2)	9.1×10^{6}	3.0×10^{7}

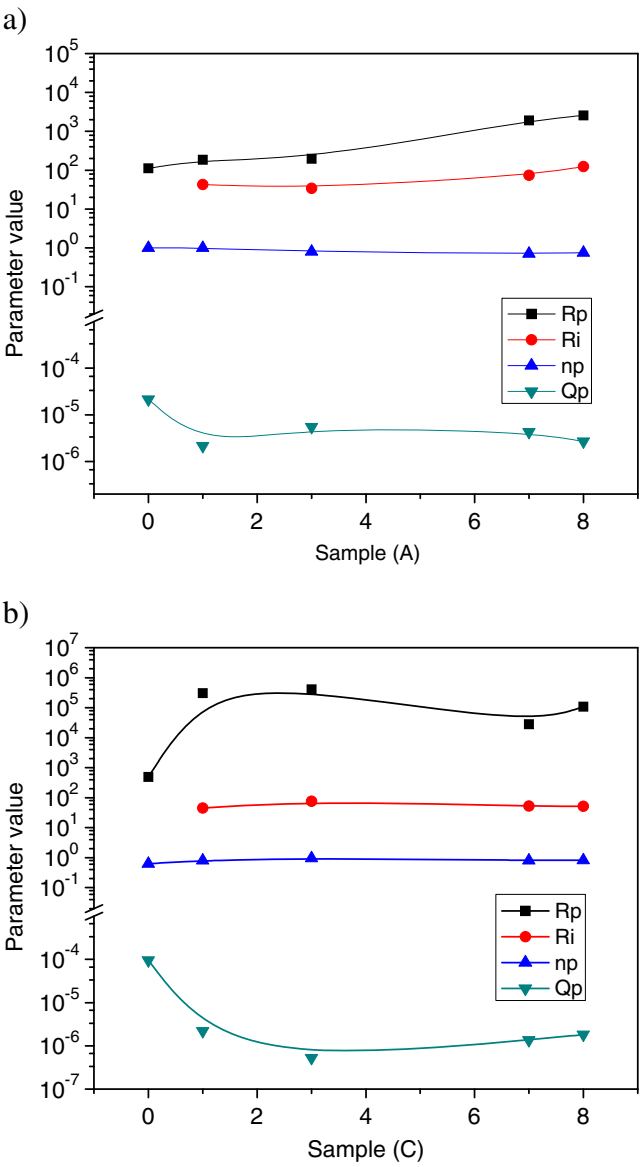

Fig. 13 Change of relevant EC parameters with working age of processing solution for **a** thermal printing plate and **b** conventional printing plate. Note the break in scale of Y-axis

both PP types. The differences in response of PP to processing discussed above are clearly seen. The narrow pores of conventional PP are quickly sealed by processing (rapid increase of R_p to a high value). Broader and shallower pores of thermal PPs are partially and gradually filled up. Initially, the resistance of the intermediate layer is compatible for both types and does not change significantly with the age of processing solution. The processing of thermal PP in old solutions (samples 7 and 8) results in a significant increase of the intermediate layer thickness and its resistance with respect to that of a conventional PP that remains practically constant. The initial decrease in respective capacitances is compliant with mechanisms discussed above. For aged solutions the process of conversion of alumina to hydrated alumina may be retarded because of the aggressive ions in the aged solution. Thus, the resistance of the porous layer decreases and the capacitance of the porous layer increase, as observed for conventional PPs (Fig. 13b, samples 7 and 8).

The results of EIS for the thermal PP and corresponding changes in resistance and capacitance values of ECs indicate that during the chemical processing the anhydrous aluminium oxide reacts with water and forms less dense voluminous hydrated oxide resulting in a sealing effect.

By aging of processing solution, the primary process on the aluminium oxide surface changes. According to observed increase of the resistance values and lowering of the corresponding capacitance values, the primary process in processing with aged solution is the sealing effect which causes degradation from optimal roughness profile and closing of the pores in the oxide structure as a consequence of the transformation of the anhydrous oxide into voluminous hydrated oxide. In addition, the re-deposition of the dissolved material from the aged solution occurs.

It is probable that both mechanisms are occurring simultaneously, but in the first stage of processing (in relatively fresh solution) the dominant process is dissolution, while in the second stage (processing in aged solution) the dominant process is sealing probably supported by the re-deposition from the solution.

Hence, it seems that in processing with fresh solution the primary process is dissolution of peaks, while with the aging of solution the re-deposition from the solution comes into play. However, there are some differences in response of different PP types to processing with aged solution: for the thermal PP samples (A) an increase of intermediate layer and pore plug resistances are noticed, while for the conventional PP (C samples) the resistances of the intermediate layer and of the pore filling do not change substantially with aging of the processing solution, thus indicating that the narrower pores of conventional PP are mostly closed in processing even with completely fresh solution.

Conclusions

We have used EIS and SEM to characterize and study the porous aluminium oxide structures of lithographic PPs and their topographical changes induced by processing. Although the processing of PP should not have adverse effects on its surface structure, we have found that the structure of the PP surface does change in processing, and that this change is related to the working age of particular processing solution.

The processing with freshly prepared solution induces relatively small structural changes, while the processing with aged solutions induced surface topography changes that impaired the quality of PP.

The observed changes in the impedance spectra were successfully modeled with EC models corresponding to the anodized layer with open pore structure and to the anodized layer with sealed pores including formation of an intermediate layer of re-deposited material.

The results of our study corroborate the notion that the observed surface structural changes are induced by two different mechanisms. The first one is the degradation and smoothening of the rough surface structure of the aluminium oxide layer by dissolution, and the second one is the chemical reaction of the aluminium oxide with alkaline solution during the chemical processing and re-deposition of the material from the aged solution. The second mechanism is probably a consequence of the reaction of anhydrous aluminium oxide structure which adsorbs water from alkaline solution resulting in a sealing process. The latter process is more pronounced for thermal PPs.

Acknowledgements This research was supported by Croatian Ministry of Science, Education and Sports grants No. 098-0982915-2899: “Organizational processes and optical interactions in condensed molecular systems” and No. 128-1201785-2228 “Development of methods for printing plate’s surface measurements”. The authors would like to thank Dr.sc. Krešimir Furić of RBI for the SEM micrographs of the samples.

References

1. Limbach PKF, Amor MP, Ball J (2003) Aluminium sheet with rough surface, Patent No.: US 6,524,768 B1
2. Hutchinson R (2001) Trans Inst Met Finish 79:57–59
3. Gobbetti O (1991) Electrochemical graining of aluminum or aluminum alloy surfaces, Patent No. US 5,064,511
4. Lin CS, Chang CC, Fu HM (2001) Mater Chem Phys 68:217–224
5. Nishino A, Masuda Y, Sawada H, Uesugi A (2004) Process for producing aluminum support for lithographic printing plate, Patent No.: US 6,682,645 B2
6. Urano T, Kohori K, Okamoto H (2004) Photosensitive lithographic printing plate and method for making a printing plate, Patent No.: US 6,689,537 B2
7. Dimogerontakis Th, Van Gils S, Ottevaere H, Thienpont H, Terryn H (2006) Surf Coat Technol 201:918–926

8. Rivetta B, Korolevaa EV, Garcia-Garcia FJ, Armstrong J, Thompson GE, Skeldon P (2011) Wear 270:204–217
9. Lizarbe R, Gonzalez JA, Lopez W, Otero E (1992) Aluminum 68:140–144
10. Suay JJ, Giménez E, Rodríguez T, Habbib K, Saura JJ (2003) Corros Sci 45:611–624
11. Gonzalez JA, Lopez V, Bautista A, Otero E, Növoa XR (1999) J Appl Electrochem 29:229–238
12. van der Linden B, Terryn H, Vereecken J (1990) J Appl Electrochem 20:798–803
13. De Laet J, Scheers J, Terryn H, Vereecken J (1993) Electrochim Acta 38:2103–2109
14. Gonzalez JA, Lopez V, Otero E, Bautista A (2000) J Electrochem Soc 147:984–990
15. Von Asten W, Kernig B, Grzemba B (2009) Litho strip and method for its manufacture Patent No.: US RE40788
16. ISO 12218:1997. Graphic technology—Process control—Offset plate making
17. ISO 12647-2:2004. Graphic technology—Process control for the production of half-tone color separations, proof and production prints: Part 2. Offset lithographic processes
18. Matsumoto H, Kita N (1984) Developing solution for light-sensitive printing plates Patent No.: US 4469776
19. Takamiya S (2006) Developing solution for heat-sensitive lithographic printing plate precursor and method for preparing lithographic printing plate, Patent No.: US 7147995
20. FOGRA Project No. 22.024, Electrochemische Untersuchungen def Oberfläche von Offsetdruckplatten zur Aufklärung der Ursachen von Farbannahmeerscheinungen an bildfreien Stellen, Fogra Report 2006
21. Boukamp BA (1989) Equivalent circuit, Users manual, second revised edition. University of Twente Enschede, Netherlands
22. PAR ZSimpWin 3.21 Copyright 1999–2004 by EChem Software, Ann Arbor, MI, USA
23. Sasaki H, Shibata S, Hatanaka T (1994) Bull Natl Grassl Res Inst 49:17–24
24. Mahovic Poljacek S, Risovic D, Furic K, Gojo M (2008) Appl Surf Sci 254:3449–3458
25. ISO 4287:1997 Geometric Product Specification (GPS). Surface texture: profile method—terms, definitions and surface texture parameters
26. Risovic D, Mahovic Poljacek S, Gojo M (2009) Appl Surf Sci 255:4283–4288
27. Risovic D, Mahovic Poljacek S, Furic K, Gojo M (2008) Appl Surf Sci 255:3063–3070
28. de Levie R (1989) J Electroanal Chem Interfacial Electrochem 261:1–9
29. Assis SL, Costa I (2006) Mater Res 9:425–429
30. Kolman DG, Scully JR (1994) J Electrochem Soc 141:2633–2641
31. Yu SY, Brodrick CW, Ryan MP, Scully JR (1999) J Electrochem Soc 146:4429–4438
32. Zhao XH, Zuo Y, Zhao JM, Xiong JP, Tang YM (2006) Surf Coat Technol 200:6864–6853
33. Hoar TP, Wood GC (1962) Electrochim Acta 7:333–353
34. Hitzig J, Juttner K, Lorenz WJ, Paatsch W (1986) J Electrochem Soc 133:887–892
35. Hitzig J, Juttner K, Lorenz WJ, Paatsch W (1984) Corros Sci 24:945–952
36. Lizarbe R, González JA, Otero E, López V (1993) Alum 69:548
37. González JA, López V, Otero E, Bautista A, Lizarbe R, Barba C, Baldonedo JL (1997) Corros Sci 39:1109–1118
38. Suay JJ, Giménez E, Rodríguez T, Habbib K, Saura JJ (2003) Corros Sci 45:611–624
39. Wood GC (1973) In: Diggle JW (ed) Oxides and oxide films, vol 2. Marcel Dekker, New York
40. Bartolomé MJ, López V, Escudero E, Caruana G, González JA (2006) Surf Coat Technol 200:4530–4537
41. Feliu S Jr, González JA, López V, Bartolome MJ, Escudero E, Otero E (2007) J Appl Electrochem 37:1027–1037
42. López V, Bartolomé MJ, Escudero E, Otero E, González JA (2006) J Electrochem Soc 153:B75–B82